

Substituent Effects in Digermanes: Electrochemical, Theoretical, and Structural Investigations

Erin K. Schrick,[†] Trevor J. Forget,[†] Kimberly D. Roewe,[†] Aaron C. Schrick,[†] Curtis E. Moore,[‡] James A. Golen,^{‡,§} Arnold L. Rheingold,[‡] Nicholas F. Materer,[†] and Charles S. Weinert^{*,†}

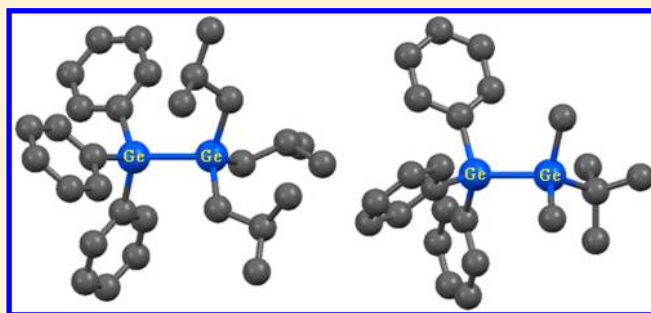
[†]Department of Chemistry, Oklahoma State University, Stillwater, Oklahoma 74078, United States

[‡]Department of Chemistry and Biochemistry, University of California San Diego, La Jolla, California 92093-0358, United States

[§]University of Massachusetts Dartmouth, North Dartmouth, Massachusetts 02747, United States

S Supporting Information

ABSTRACT: The digermanes $R_3GeGePh_3$ ($R_3 = Bu^i_3$, Hex^n_3 , $(C_{18}H_{37})_3$, or Bu^iMe_2) were synthesized using the hydrogermylation reaction, and the X-ray crystal structures of $Bu^i_3GeGePh_3$ and $Bu^iMe_2GeGePh_3$ were determined. The isobutyl-substituted digermane contains two independent molecules in the unit cell with Ge–Ge bond distances of 2.4410(5) and 2.4409(5) Å, and $Bu^iMe_2GeGePh_3$ has a Ge–Ge bond distance of 2.4255(3) Å. These four digermanes and the four additional digermanes $R_3GeGePh_3$ ($R_3 = Me_3$, Bu^n_3 , Bu^s_3 , or $PhMe_2$) were characterized by cyclic voltammetry, differential pulse voltammetry, and linear sweep voltammetry in order to determine the effects of varying substituent patterns on the oxidation potential of these systems. Digermanes having more inductively donating substituents exhibit more negative oxidation potentials than those having less inductively donating substituents. Density functional theory calculations were also performed on these eight systems, and the energies of their frontier orbitals were determined. The energy of the HOMO and LUMO in these systems was shown to depend on the electron-donating ability of the organic substituents.



INTRODUCTION

Oligogermanes are a class of catenated compounds that structurally resemble saturated hydrocarbons but possess physical properties that more closely mirror those of conjugated unsaturated polyenes.^{1–3} However, as opposed to these π -conjugated organic systems, oligogermanes exhibit σ -delocalization, where the pair of electrons present in the highest occupied molecular orbital (HOMO) are delocalized across the germanium–germanium backbone, provided that the germanium atoms are coplanar and are arranged in a sequential *trans*-conformation.^{4,5} Therefore, these molecules can exhibit $\sigma \rightarrow \sigma^*$ electronic transitions that are similar to the $\pi \rightarrow \pi^*$ transitions observed in their doubly or triply bonded carbon congeners, resulting in the observation of broad but distinct absorbance peaks in their UV/visible spectra. The σ -bonding electrons present in these molecules have also been shown to interact with the available π or π^* molecular orbitals on aryl substituents attached to the Ge–Ge backbone, which shifts their observed λ_{max} values to lower energy.^{6–10} Oligogermanes are also electrochemically active, and their oxidation potentials can be readily obtained using cyclic voltammetry or differential pulse voltammetry.^{9–15} The majority of these compounds exhibit a single irreversible oxidation wave, although aryl-substituted linear oligogermanes have been shown to undergo $n - 1$

sequential oxidation steps, where n is the number of catenated germanium atoms.^{10,13}

We have developed a versatile method for the construction of singly bonded oligogermanes that makes use of the hydrogermylation reaction as the key step in Ge–Ge bond formation.^{7–10,13,14,16,17} This reaction proceeds in acetonitrile solvent, which also doubles as a key synthetic reagent, as it is involved in the conversion of the germanium amide starting material R_3GeNMe_2 into an α -germyl nitrile R_3GeCH_2CN , which is the active species in the Ge–Ge bond-forming process. The hydrogermylation reaction can be coupled with a hydride protection/deprotection strategy that allows for sequential chain buildup where the germanium atoms are added to the chain one at a time. Using these methods, we are able to control both the degree of catenation and the substituent pattern, which was not possible using other previously developed synthetic techniques.

We have characterized the majority of the oligogermanes prepared in our laboratory using UV/visible spectroscopy and cyclic voltammetry and have established a correlation between the structures of these materials and their physical properties. The energy of the HOMO–LUMO gap in these compounds

Received: February 14, 2013

Published: March 18, 2013

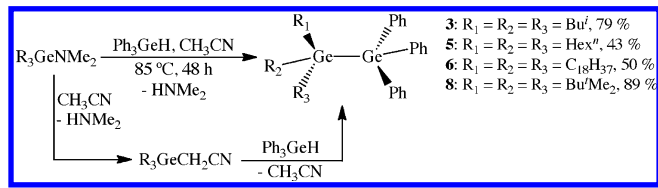
decreases with an increase in the number of catenated germanium atoms and also with the incorporation of more inductively donating organic substituents along the Ge–Ge backbone.^{7,9} Variation of the degree of catenation has a more prolific effect on the energies of the frontier orbitals in these compounds than does variation of the substituents, but changes in the substituent pattern do have a measurable effect.

In order to investigate the substituent effects on the oxidation potentials of these systems in detail, we have investigated a series of digermanes having the general formula $R_3\text{GeGePh}_3$ ($R_3 = \text{Me}_3$ (1),^{6,18,19} Bu^i_3 (2),¹⁷ Bu^s_3 (3), Bu^t_3 (4),²⁰ Hex^n_3 (5), $(\text{C}_{18}\text{H}_{37})_3$ (6), PhMe_2 (7),²⁰ or Bu^tMe_2 (8)), where compounds 3, 5, 6, and 8 are newly synthesized. Digermanes are the simplest systems containing single Ge–Ge bonds, and the substituents are varied at only one of the germanium atoms in the series of digermanes at hand. We have found that more inductively electron-donating substituents destabilize the HOMO in these molecules and therefore render them easier to oxidize, and these effects are somewhat subtle. For example, different oxidation potentials were observed for the three isomeric butyl-substituted species 2–4. We have also combined our electrochemical investigations with density functional theory calculations that were used to determine the energies of the frontier orbitals in these systems. We have found excellent correlation between the experimental and theoretical data, and these results are described below.

RESULTS AND DISCUSSION

The newly synthesized digermanes 3, 5, 6, and 8 were prepared according to Scheme 1, and the corresponding germanium

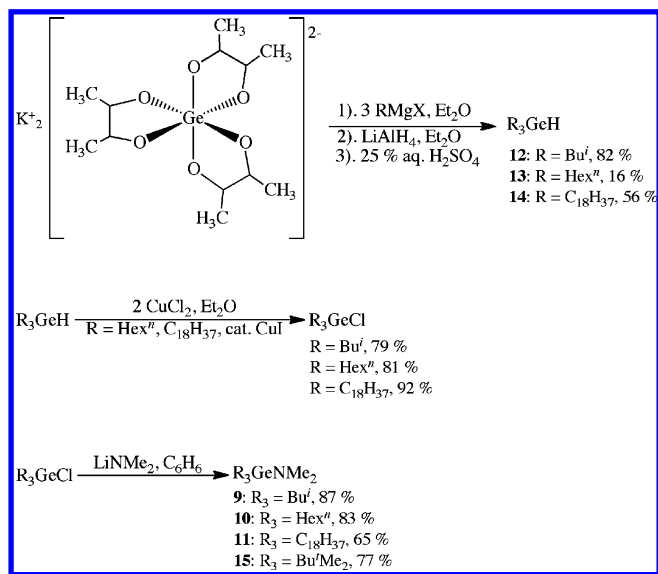
Scheme 1



amides used for their synthesis ($\text{Bu}^i_3\text{GeNMe}_2$ (9), $\text{Hex}^n_3\text{GeNMe}_2$ (10), and $(\text{C}_{18}\text{H}_{37})_3\text{GeNMe}_2$ (11)) were prepared in four steps starting from GeO_2 . A significant limitation in the area of oligogermane chemistry is the lack of reliable preparative routes for the synthesis of organogermane starting materials having the general formula $R_3\text{GeX}$ or $R_2\text{GeX}_2$ ($R = \text{an alkyl or aryl group, } X = \text{Cl or Br}$). However, triorganogermane compounds $R_3\text{GeH}$ can be readily prepared by the method of Corriu et al.,^{21,22} and we have used this preparative route for the synthesis of the three germanium starting materials Bu^i_3GeH (12), Hex^n_3GeH (13; $\text{Hex}^n = n\text{-C}_6\text{H}_{13}$), and $(\text{C}_{18}\text{H}_{37})_3\text{GeH}$ (14), none of which are commercially available (Scheme 2). An important advantage of this method is that it makes use of the inexpensive starting material GeO_2 instead of GeCl_4 or GeBr_4 , which are typically used in other preparative routes.

The three newly synthesized organogermanes 12–14 each exhibit a characteristic Ge–H resonance in their ^1H NMR spectra. These were observed as septets at 3.53 (12), 4.08 (13), and 4.00 (14) ppm with $^3J_{\text{H-H}}$ coupling constants of 2.8 (12), 3.0 (13), and 2.7 (14) Hz. These compounds also exhibit sharp $\nu_{\text{Ge-H}}$ stretching bands in their infrared spectra at 2100 (12), 2005 (13), and 2007 (14) cm^{-1} , which are observed at lower energy than those for Ph_3GeH and Mes_3GeH ($\text{Mes} = 2,4,6\text{-trimethylphenyl}$) at

Scheme 2



2037 and 2033 cm^{-1} , respectively,²³ since 12–14 contain alkyl rather than aryl substituents. Both 12 and 13 are liquids, while the octadecyl derivative 14 is a solid at room temperature. The three organogermanes were converted to the corresponding chlorides via the method of Kunai et al.²⁴ and subsequently to the amides 9–11 by salt metathesis with LiNMe_2 (Scheme 2). The ^1H NMR spectra of the three amide compounds contained a singlet for their $-\text{N}(\text{CH}_3)_2$ protons at 2.57 (9), 2.65 (10), and 2.64 (11) ppm. The amide $\text{Bu}^t\text{Me}_2\text{GeNMe}_2$ (15) was synthesized from commercially available $\text{Bu}^t\text{Me}_2\text{GeCl}$ and exhibits a resonance at 2.60 ppm corresponding to its $-\text{N}(\text{CH}_3)_2$ protons.

The amides 9–11 and 15, as well as the previously reported amides $R_3\text{GeNMe}_2$ ($R_3 = \text{Me}_3$,²⁵ Bu^i_3 ,¹⁷ Bu^s_3 ,²⁰ PhMe_2 ,²⁰), were treated with Ph_3GeH in acetonitrile solvent to yield the digermanes 1–8. This reaction proceeds via the *in situ* conversion of the germanium amide starting materials $R_3\text{GeNMe}_2$ to the corresponding α -germyl nitriles $R_3\text{GeCH}_2\text{CN}$, as shown in Scheme 1.^{16,17} All of the digermanes synthesized are crystalline solids, with the exception of the trihexyl-substituted derivative 5, which is a viscous clear liquid, and the octadecyl-substituted digermane 6, which is an oily solid. The new digermanes 3, 5, 6, and 8 were characterized by NMR (^1H and ^{13}C) spectroscopy and elemental analysis, and the X-ray crystal structures of 3 and 8 were also determined.

The ^1H NMR spectrum of $\text{Bu}^i_3\text{GeGePh}_3$ (3) contains the expected pattern for the three isobutyl groups with two doublets at 0.88 ($J = 6.6$ Hz) and 1.25 ($J = 6.6$ Hz) ppm corresponding to the methylene and methyl protons as well as a multiplet at 1.90 ppm corresponding to the methine protons. The ^1H NMR spectrum for $\text{Bu}^t\text{Me}_2\text{GeGePh}_3$ (8) contains two singlets at 2.60 and 0.97 ppm arising from the protons of the *tert*-butyl group and the methyl groups, respectively. The chemical shift for the methyl groups of 8 differs from that for the signal corresponding to the related phenyl-substituted derivative $\text{PhMe}_2\text{GeGePh}_3$ (7)²⁰ observed at 0.64 ppm. The upfield shift of the methyl group protons in 7 versus those of 8 can be attributed to through-space shielding of these protons by the π -electron cloud of the phenyl ring in 7,^{26,27} which is absent in the *tert*-butyl-substituted derivative 8.

The ^1H NMR spectrum of $\text{Hex}^n_3\text{GeGePh}_3$ (5) contains several overlapping resonances for the methylene protons of

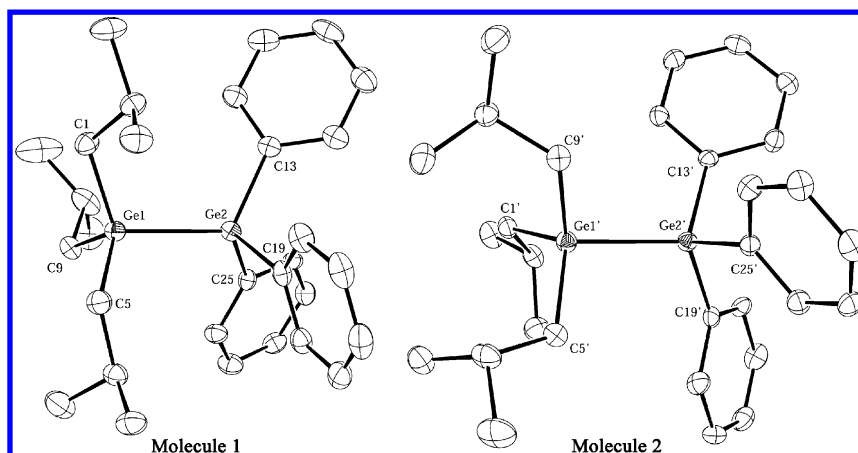


Figure 1. ORTEP diagram of $\text{Bu}_3\text{GeGePh}_3$ (**3**). Thermal ellipsoids are drawn at 50% probability.

the *n*-hexyl group, but the ^{13}C NMR spectrum contains six distinct resonances at 32.3, 31.9, 26.7, 23.0, 14.3, and 12.5 ppm. The resonances are arranged in a progressing upfield pattern based on their proximity to the germanium atom, with the feature at 32.3 ppm corresponding to the α -carbon atom, while that at 12.5 ppm is due to the terminal methyl group. Similarly, the ^1H NMR spectrum of $(\text{C}_{18}\text{H}_{37})_3\text{GeGePh}_3$ (**6**) contains a single intense broad feature at 1.34 ppm arising from the 17 groups of methylene protons and a triplet at 0.91 ppm ($J = 6.6$ Hz) corresponding to the terminal methyl group. The ^{13}C NMR spectrum of **6** contains a single intense resonance at 30.3 ppm arising from 14 of the 18 carbon atoms present in the octadecyl chain. Additional features were also observed and correspond to the α - CH_2 carbon atom (23.2 ppm), the two carbon atoms of the methylene groups proximal to the octadecyl chain terminus (32.4 and 29.9 ppm), and the terminal methyl group (14.4 ppm). A similar chemical shift pattern was reported for the germane $\text{Bu}^n_3\text{Ge}(\text{C}_{11}\text{H}_{23})$.²⁸

The X-ray crystal structures of **3** and **8** have been determined, and ORTEP diagrams are shown in Figures 1 and 2, respectively. Selected bond distances and angles are also

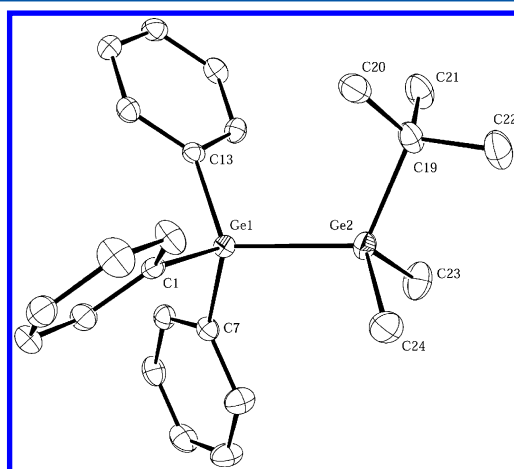


Figure 2. ORTEP diagram of $\text{Bu}^4\text{Me}_2\text{GeGePh}_3$ (**8**). Thermal ellipsoids are drawn at 50% probability.

collected in Tables 1 (**3**) and 2 (**8**). The triisobutyl-substituted digermane **3** crystallizes with two independent molecules in the unit cell, having germanium–germanium bond distances of

Table 1. Selected Bond Distances (Å) and Angles (deg) for $\text{Bu}_3\text{GeGePh}_3$ (**3**)

	molecule 1	molecule 2	average	
Ge(1)–Ge(2)	2.4410(5)	Ge(1')–Ge(2')	2.4409(5)	2.4410(5)
Ge(1)–C(1)	1.962(3)	Ge(1')–C(1')	1.972(3)	1.967(3)
Ge(1)–C(5)	1.972(4)	Ge(1')–C(5')	1.975(4)	1.974(4)
Ge(1)–C(9)	1.970(3)	Ge(1')–C(9')	1.985(4)	1.978(4)
Ge(2)–C(13)	1.956(4)	Ge(2')–C(13')	1.957(4)	1.957(4)
Ge(2)–C(19)	1.957(4)	Ge(2')–C(19')	1.952(3)	1.955(4)
Ge(2)–C(25)	1.958(3)	Ge(2')–C(25')	1.968(3)	1.963(3)
C(1)–Ge(1)–C(5)	109.3(2)	C(1')–Ge(1')–C(5')	116.0(2)	112.7(2)
C(1)–Ge(1)–C(9)	109.5(2)	C(1')–Ge(1')–C(9')	110.0(1)	109.8(2)
C(5)–Ge(1)–C(9)	112.8(2)	C(5')–Ge(1')–C(9')	112.0(2)	112.4(2)
C(13)–Ge(2)–C(19)	106.4(2)	C(13')–Ge(2')–C(19')	109.6(1)	108.0(2)
C(13)–Ge(2)–C(25)	106.5(1)	C(13')–Ge(2')–C(25')	106.7(1)	106.6(1)
C(19)–Ge(2)–C(25)	106.9(2)	C(19')–Ge(2')–C(25')	106.4(1)	106.6(2)
C(1)–Ge(1)–Ge(2)	110.5(1)	C(1')–Ge(1')–Ge(2')	112.2(9)	111.4(1)
C(5)–Ge(1)–Ge(2)	106.7(1)	C(5')–Ge(1')–Ge(2')	102.63(9)	104.7(7)
C(9)–Ge(1)–Ge(2)	107.9(1)	C(9')–Ge(1')–Ge(2')	103.2(1)	105.5(1)
C(13)–Ge(2)–Ge(1)	115.72(9)	C(13')–Ge(2')–Ge(1')	110.94(9)	113.33(9)
C(19)–Ge(2)–Ge(1)	108.0(1)	C(19')–Ge(2')–Ge(1')	115.1(1)	111.5(1)
C(25)–Ge(2)–Ge(1)	112.84(9)	C(25')–Ge(2')–Ge(1')	107.63(9)	110.24(9)

Table 2. Selected Bond Distances (Å) and Angles (deg) for $\text{Bu}^4\text{Me}_2\text{GeGePh}_3$ (**8**)

Ge(1)–Ge(2)	2.4255(3)	C(19)–Ge(2)–C(23)	108.02(9)
Ge(1)–C(1)	1.952(2)	C(19)–Ge(2)–C(24)	109.93(9)
Ge(1)–C(7)	1.962(2)	C(23)–Ge(2)–C(24)	107.8(1)
Ge(1)–C(13)	1.949(2)	Ge(1)–Ge(2)–C(19)	115.27(6)
Ge(2)–C(19)	1.989(2)	Ge(1)–Ge(2)–C(23)	107.37(7)
Ge(2)–C(23)	1.951(2)	Ge(1)–Ge(2)–C(24)	108.18(6)
Ge(2)–C(24)	1.951(2)	Ge(2)–Ge(1)–C(1)	110.51(5)
C(1)–Ge(1)–C(7)	106.73(7)	Ge(2)–Ge(1)–C(7)	109.05(5)
C(1)–Ge(1)–C(13)	110.73(7)	Ge(2)–Ge(1)–C(13)	112.91(5)
C(7)–Ge(1)–C(13)	106.63(8)		

2.4410(5) and 2.4409(5) Å and an average distance of 2.4410(5) Å. The Ge–Ge bond distance in **3** is longer than the 2.4208(8) Å Ge–Ge bond distance in the *n*-butyl-substituted analogue $\text{Bu}^n_3\text{GeGePh}_3$ (**2**)¹⁷ due to the increased steric effects of the branching present at the β -carbon of the three isobutyl groups in **3**. The Ge–Ge bond distance in **3** is also elongated relative to those in $\text{Me}_3\text{GeGePh}_3$ (**1**)¹⁸ and $\text{Et}_3\text{GeGePh}_3$,¹⁷ which measure 2.418(1) and 2.4253(7) Å, respectively, despite the fact that the structures of **1** and

$\text{Et}_3\text{GeGePh}_3$ are C_3 -symmetric, where the alkyl and phenyl groups on the two germanium atoms are in an eclipsed conformation. However, the Ge–Ge bond distance in **3** is shorter than those in the more sterically encumbered digermanes $\text{Ph}_3\text{GeGePh}_3$,²⁹ and $\text{Pr}_3^i\text{GeGePh}_3$,¹⁶ which measure 2.446(1) and 2.4637(7) Å, respectively.

The increased steric effects of the isobutyl substituent are also manifested in the Ge– C_α bond distances, which average 1.973(5) Å in **3** and are longer than the average bond distance of 1.951(6) Å in **2**.¹⁷ The average C–Ge–C bond angle about the Ge(1) is 111.6(2)°, while in **2** the corresponding bond angle is 108.6(2)°, and the average C_α –Ge–Ge bond angles in **3** and **2** are 107.2(1)° and 110.3(2)°, respectively. The more significant deviation from an idealized tetrahedral environment in **3** is again a result of the increased steric attributes of the isobutyl substituents versus the *n*-butyl substituents in **2**.

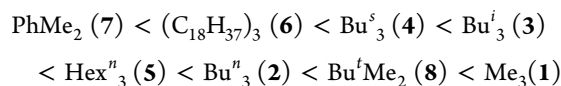
The Ge–Ge bond distance in $\text{Bu}^i\text{Me}_2\text{GeGePh}_3$ (**8**) is 2.4255(3) Å and is only slightly longer than that in $\text{PhMe}_2\text{GeGePh}_3$ (**7**) (2.4216(4) Å)²⁰ but is nearly identical to the Ge–Ge bond distance in $\text{Me}_3\text{GeGePh}_3$ (**1**) of 2.418(1) Å.¹⁸ Thus, the replacement of a single methyl group with either a *tert*-butyl or phenyl substituent has little effect on the Ge–Ge bond distance among these three molecules. The Ge(1)–C(19) bond distance to the central carbon atom of the *tert*-butyl group is 1.989(2) Å, which is longer than typical Ge–C bond distances of 1.95–1.97 Å as a result of the steric encumbrance of the *tert*-butyl group. The average C–Ge–C bond angle about Ge(2) is 108.6(1)°, which is close to the ideal tetrahedral bond angle and is also similar to the related C–Ge–C bond angles in **7** (109.2(2)°) and **1** (108.7(1)°).

Variation of the substituents at the alkyl-substituted germanium atom has a minimal effect on the geometry at the second phenyl-substituted germanium atom. The environment about the phenyl-substituted germanium atom in the five crystallographically characterized digermanes **1–3**, **7**, and **8** is essentially identical, with average Ge– C_{ipso} bond distances falling into the narrow range 1.955(4)–1.958(4) Å and the average C_{ipso} –Ge– C_{ipso} bond angles in the range 107.1(2)–108.7(2)°. The substituents on the two germanium atoms adopt a staggered conformation in compounds **2**, **3**, **7**, and **8**, while in **1**¹⁸ and $\text{Et}_3\text{GeGePh}_3$ ¹⁷ the conformations are eclipsed.

The digermanes **1–8** were each characterized using cyclic voltammetry (CV), differential pulse voltammetry (DPV), and linear sweep voltammetry (LSV), and the experimental results are collected in Table 3. A representative overlaid CV and DPV

The cyclic and differential pulse voltammograms, as well as the linear sweep voltammograms, of the other seven digermanes are nearly identical in appearance. The CV of **3** shown in Figure 3 contains a single irreversible oxidation wave at 1510 ± 9 mV, while the DPV contains an anodic current peak at 1410 ± 7 mV and the LSV contains an oxidation wave at 1545 ± 13 . The oxidation waves for **1–8** in their CVs all appear at higher potential than those in the corresponding DPVs, as expected since the charging current present in the CV is suppressed in the DPV experiment. In addition, the DPV oxidation waves appear at the same potential within experimental error when the voltammograms are acquired with the potential progressing in either the positive or negative direction. The 10-cycle CV of **3** shown in Figure 5 is also nearly identical in appearance to those for the other seven digermanes. The position of the oxidation wave remains at the same potential within experimental error for each cycle, and the anodic current diminishes slightly with each progressive scan.

The trend in oxidation potentials in these digermanes, from easiest to most difficult to oxidize and based on their varying substituents, is as follows:



Of the eight digermanes investigated, the trimethyl-substituted species **1** is the most difficult to oxidize, having a single irreversible oxidation wave in its cyclic voltammogram at 1795 mV, while the most facile digermane to oxidize is $\text{PhMe}_2\text{GeGePh}_3$ (**7**), which exhibits an oxidation wave at 1450 mV. The digermane **1** lacks the more electron-donating substituents present in **2–6**, and therefore **1** is expected to be the most difficult to oxidize. The same trend in electron-donating ability of the substituents and oxidation potential is maintained in the series of three digermanes $\text{Me}_3\text{GeGePh}_3$ (**1**), Bu^iMe_2 (**8**), and PhMe_2 (**7**). Substituting a methyl group in **1** for a *tert*-butyl group in **8** diminishes the oxidation potential of **8** by ca. 195 mV versus that for **1**, while the oxidation potential of **7** is ca. 345 mV more negative than that of **1**. The Bu^t group in **8** is more inductively electron donating than a methyl group, and thus the energy of the HOMO, which is taken to be the source of the electron removed from the digermane upon oxidation, should be destabilized in **8** versus **1**.

Although the *ipso*-carbon atom of the phenyl group present in **7** is effectively more electronegative and therefore less electron donating than that of a germanium-bound alkyl substituent, the π -system of the phenyl group serves as an electron donor to the germanium atom and destabilizes the HOMO of **7** relative to those in both **8** and **1**, and thus **7** is the most facile of these three compounds (and the most facile overall) to oxidize.

This same trend is also observed among the three digermanes $\text{Bu}^n_3\text{GeGePh}_3$ (**2**), $\text{Hex}^n_3\text{GeGePh}_3$ (**5**), and $(\text{C}_{18}\text{H}_{37})_3\text{GeGePh}_3$ (**6**). The *n*-butyl-substituted digermane **2** is the most difficult to oxidize, while the *n*-hexyl derivative **5** has an oxidation potential that is ca. 45 mV more negative than that of **2** and that for the octadecyl-substituted digermane **6** is ca. 25 mV more negative than that of **5**. Furthermore, although the values are very similar when considering experimental error, the expected trend is also observed among the three tributyl-substituted digermanes $\text{Bu}^s_3\text{GeGePh}_3$ (**4**), $\text{Bu}^i_3\text{GeGePh}_3$ (**3**), and $\text{Bu}^n_3\text{GeGePh}_3$ (**2**), where the *n*-butyl digermane **2** is the most difficult to oxidize and the *sec*-butyl digermane **4** is the

Table 3. Electrochemical Data for Digermanes 1–8

compound	CV (mV) ^a	DPV (mV) ^b	LSV (mV) ^c
$\text{Me}_3\text{GeGePh}_3$ (1)	1795 ± 11	1605 ± 8	1802 ± 12
$\text{Bu}^n_3\text{GeGePh}_3$ (2)	1550 ± 12	1540 ± 9	1532 ± 11
$\text{Bu}^i_3\text{GeGePh}_3$ (3)	1510 ± 10	1410 ± 9	1545 ± 13
$\text{Bu}^s_3\text{GeGePh}_3$ (4)	1505 ± 12	1405 ± 7	1535 ± 10
$\text{Hex}^n_3\text{GeGePh}_3$ (5)	1515 ± 11	1410 ± 8	1510 ± 10
$(\text{C}_{18}\text{H}_{37})_3\text{GeGePh}_3$ (6)	1490 ± 13	1400 ± 11	1485 ± 14
$\text{PhMe}_2\text{GeGePh}_3$ (7)	1450 ± 9	1330 ± 7	1445 ± 12
$\text{Bu}^t\text{Me}_2\text{GeGePh}_3$ (8)	1600 ± 8	1470 ± 7	1610 ± 11

^aConditions: 0.1 M $[\text{Bu}^n_4\text{N}][\text{PF}_6]$, scan rate = 100 mV/s. ^bConditions: 0.1 M $[\text{Bu}^n_4\text{N}][\text{PF}_6]$, pulse period = 0.1 s, pulse width = 0.05 s. ^cConditions: 0.1 M $[\text{Bu}^n_4\text{N}][\text{PF}_6]$, scan rate = 100 mV/s.

of **3** is shown in Figure 3, an LSV of $\text{Bu}^i_3\text{GeGePh}_3$ (**3**) is shown in Figure 4, and a 10-cycle CV scan of **3** is shown in Figure 5.

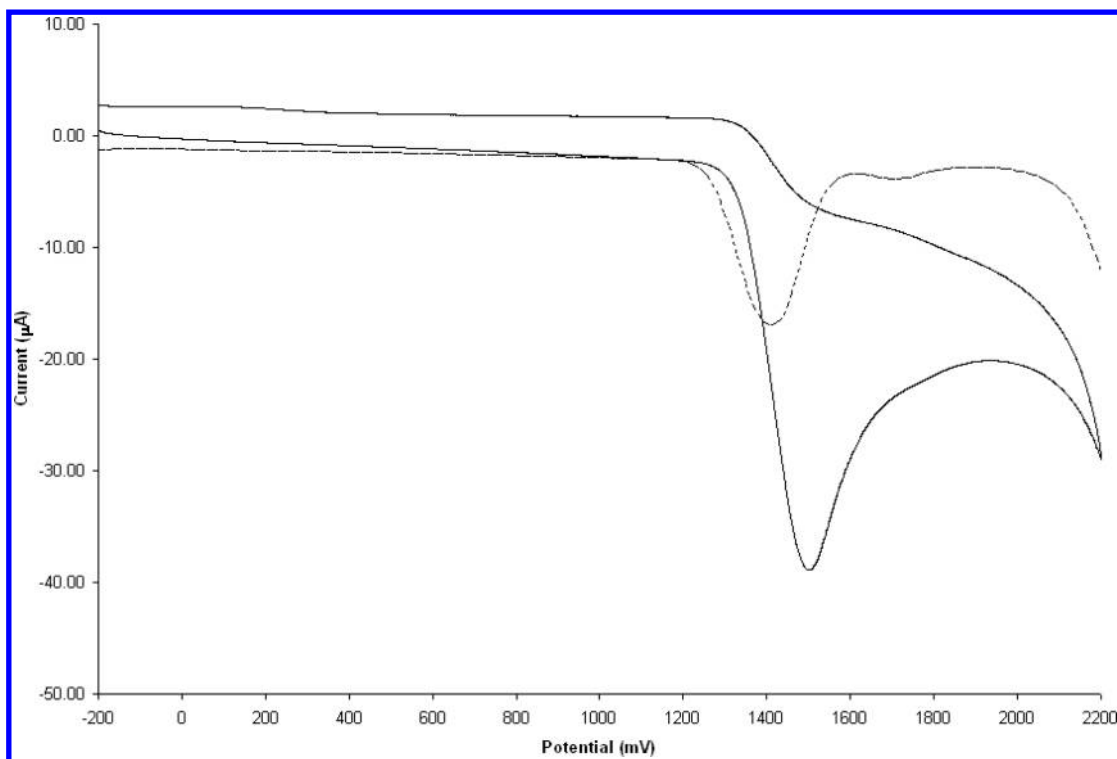


Figure 3. CV (scan rate = 100 mV/s) and DPV (pulse period = 0.1 s, pulse width = 0.05 s, sample time = 0.02 s) of $\text{Bu}_3\text{GeGePh}_3$ (**3**) in CH_2Cl_2 solvent with 0.1 M $[\text{Bu}_4\text{N}][\text{PF}_6]$ as the supporting electrolyte.

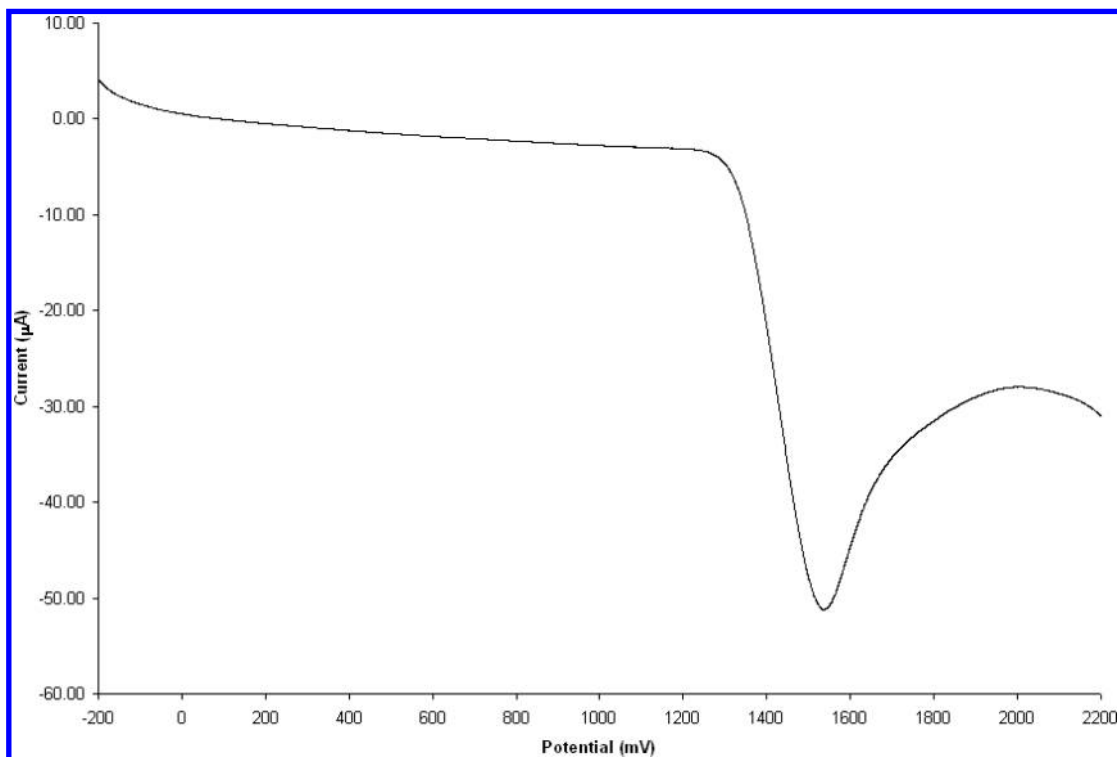


Figure 4. LSV of $\text{Bu}_3\text{GeGePh}_3$ (**3**) in CH_2Cl_2 solvent with 0.1 M $[\text{Bu}_4\text{N}][\text{PF}_6]$ as the supporting electrolyte. Sweep rate = 100 mV/s.

least difficult. This trend also correlates with the values calculated for the inductive substituent constant σ_I for these groups.³⁰ The values of σ_I for an *n*-butyl, isobutyl, and *sec*-butyl group are 0.0617, 0.0635, and 0.0688, respectively.

Although we^{10,13} and others^{11,12} have observed only irreversible oxidation waves in the cyclic voltammograms of

these species, a concrete reason for the absence of a reversible or quasi-reversible process has not been offered. The irreversibility of the oxidations of oligogermanes suggests that a chemical reaction is occurring after the oligogermane is oxidized. We have postulated that germylene extrusion might be occurring that results in concomitant chain contraction,

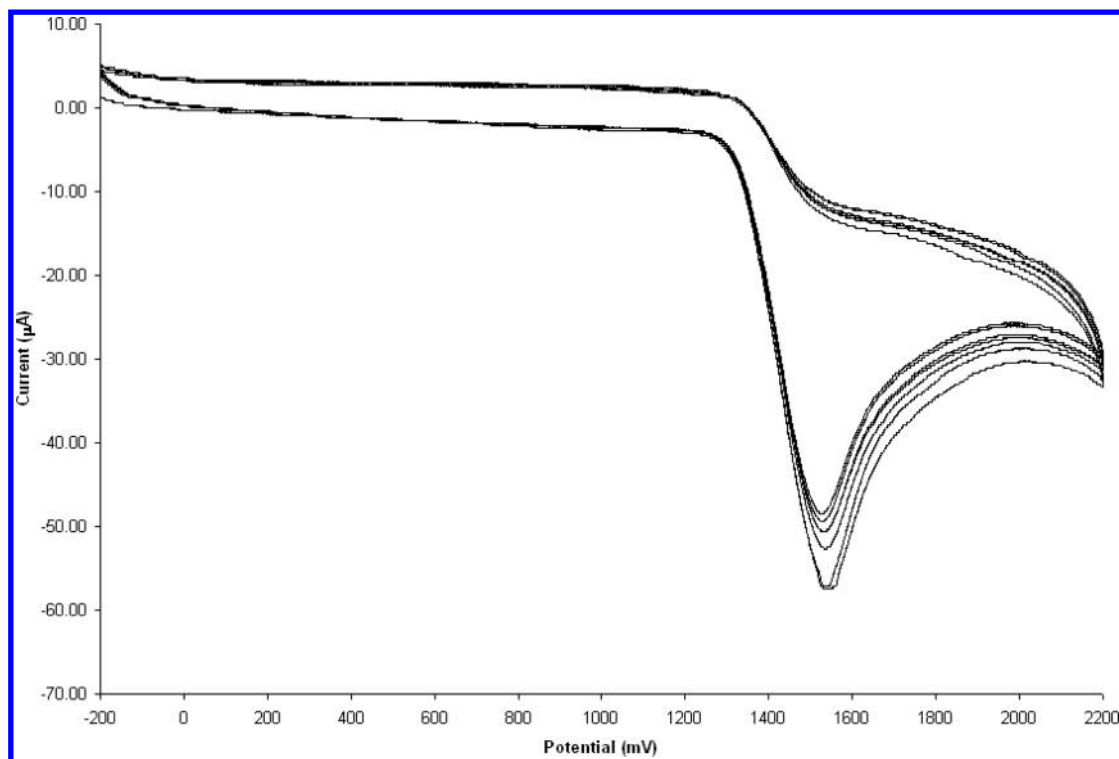
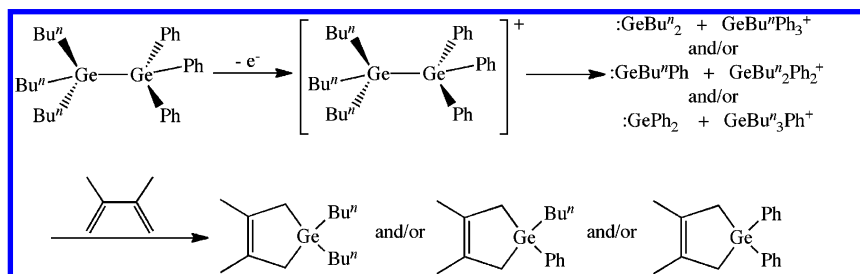


Figure 5. Ten-cycle CV of $\text{Bu}_3\text{GeGePh}_3$ (**3**) in CH_2Cl_2 solvent with 0.1 M $[\text{Bu}_4\text{N}][\text{PF}_6]$ as the supporting electrolyte.

Scheme 3



particularly since we have observed $n - 1$ oxidation waves of aryl-substituted oligogermanes having the general formula $\text{Ge}_n\text{Ar}_{2n+2}$.^{10,13} Further evidence for the possibility of germylene extrusion stems from UV irradiation of oligogermanes in the presence of the trapping reagent CCl_4 or 2,3-dimethyl-1,3-butadiene, leading to the isolation of R_2GeCl_2 or 1,1-dialkyl-3,4-dimethyl-1-germacyclopent-3-ene, although the formation of germanium radicals resulting from homolytic scission of the Ge–Ge bonds was also detected as a competing process.^{31–38} These investigations included the photolysis of the digermanes $\text{PhMe}_2\text{GeGeMe}_3$ ³⁸ and $\text{PhMe}_2\text{GeGeMe}_2\text{Ph}$,³⁵ which resulted in the detection of germylenes and germynyl radicals.

In order to attempt to ascertain if germylene extrusion is the process occurring after oxidation of the digermanes, we conducted bulk electrolysis experiments on $\text{Bu}_3\text{GeGePh}_3$ (**2**) in the presence of ca. 20 equiv of 1,3-dimethylbutadiene, which was expected to yield one or more of the trapping products shown in Scheme 3. Electrolysis of a 0.500 g sample of **2** over a 4 h period at a potential of 2100 mV was carried out in dichloromethane. The current reached a plateau after 84 min, the resulting mixture was evaporated to dryness, and the products were extracted from the crude reaction mixture with hexane. Evaporation of the hexane yielded a solid material that

was characterized by NMR (^1H and ^{13}C) spectroscopy. However, there was no evidence for the formation of any of the three possible trapping products shown in Scheme 3.^{39,40}

In order to obtain a better understanding of the electronic makeup of these molecules, density functional theory calculations were performed on **1–8** using the 6-311G(d,p) basis set.⁴¹ The energies of the frontier orbitals as well as the calculated UV/visible absorbance maxima, experimental λ_{max} values, and CV oxidation potentials of these eight species are collected in Table 4. These data are arranged in order of increasing stabilization of the HOMO. The HOMO for **1** is the most stabilized at -6.402 eV, while that for the *sec*-butyl derivative **4** is the most destabilized at -6.277 eV, and the HOMO energies among these eight digermanes lie within 0.125 eV of one another.

The energy ordering shown in Table 4 deviates somewhat from the order described above for the oxidation potentials of these eight digermanes, but this is expected due to the proximity in energy of the HOMO in these compounds. We presume that the electron removed from the digermanes during oxidation lies in the HOMO, although there are contributions to this molecular orbital other than those involved in formation of the germanium–germanium bond. In particular, the phenyl

Table 4. Computational and Experimental Data for Digermanes 1–8

compound	HOMO (eV)	LUMO (eV)	HOMO–LUMO gap (nm)	theor λ_{\max} (nm) ^a	transition	λ_{\max} (nm)	E_{ox} (mV) ^b
Bu ⁱ ₃ GeGePh ₃ (4)	−6.277	−0.804	227	242 (0.0845)	HOMO → LUMO+3	244	1505 ± 12
				249 (0.0684)	HOMO → LUMO+2		
				252 (0.0541)	HOMO → LUMO+1		
				257 (0.0441)	HOMO → LUMO		
(C ₁₈ H ₃₇) ₃ GeGePh ₃ (6)	−6.296	−0.761	224	241 (0.0530)	HOMO → LUMO+3	236	1490 ± 13
				247 (0.0682)	HOMO → LUMO+2		
				249 (0.0724)	HOMO → LUMO+1		
				240 (0.0681)	HOMO → LUMO+3		
Hex ⁿ ₃ GeGePh ₃ (5)	−6.308	−0.770	224	247 (0.0710)	HOMO → LUMO+2	241	1515 ± 11
				249 (0.0690)	HOMO → LUMO+1		
				247 (0.0679)	HOMO → LUMO+2		
				249 (0.0723)	HOMO → LUMO+1		
Bu ⁿ ₃ GeGePh ₃ (2)	−6.316	−0.768	224	251 (0.1693)	HOMO → LUMO+1	244	1450 ± 9
				258 (0.0856)	HOMO → LUMO		
				244 (0.0520)	HOMO → LUMO+2		
				249 (0.0604)	HOMO → LUMO+1		
PhMe ₂ GeGePh ₃ (7)	−6.324	−0.902	229	245 (0.0813)	HOMO → LUMO+2	238	1600 ± 8
				248 (0.0517)	HOMO → LUMO+1		
				238 (0.0739)	HOMO → LUMO+3		
				245 (0.0680)	HOMO → LUMO+2		
Bu ^t ₃ GeGePh ₃ (3)	−6.350	−0.788	223	246 (0.0679)	HOMO → LUMO+1	230	1795 ± 11
				249 (0.0604)	HOMO → LUMO+1		
				248 (0.0517)	HOMO → LUMO+1		
				245 (0.0680)	HOMO → LUMO+2		
Bu ^t Me ₂ GeGePh ₃ (8)	−6.370	−0.825	224	244 (0.0520)	HOMO → LUMO+2	232	1510 ± 10
				249 (0.0604)	HOMO → LUMO+1		
				245 (0.0813)	HOMO → LUMO+2		
				248 (0.0517)	HOMO → LUMO+1		
Me ₃ GeGePh ₃ (1)	−6.402	−0.821	222	244 (0.0520)	HOMO → LUMO+2	232	1510 ± 10
				249 (0.0604)	HOMO → LUMO+1		
				245 (0.0813)	HOMO → LUMO+2		
				248 (0.0517)	HOMO → LUMO+1		

^aOscillator strengths for the individual transitions are given in parentheses. ^bValues are from cyclic voltammetry.

group on the second germanium in 7 is expected to interact with the orbitals involved in Ge–Ge bonding and therefore destabilize the HOMO, which was found in the DFT computations.

The digermanes 1 and 8 have the most stabilized HOMOs among these eight molecules, which correlates with the electrochemical results, and 4 and 6 have the most destabilized HOMOs, which also correlates with the electrochemistry data. In addition, the inductive donating effects of longer chain alkyl groups are expected to be enhanced relative to shorter chain substituents, and this is clearly indicated among the three digermanes 2, 5, and 6. The *n*-butyl-substituted digermane 2 is more difficult to oxidize than the *n*-hexyl-substituted species 5, which are both in turn more difficult to oxidize than the octadecyl 6 substituted digermane.

Time-dependent DFT calculations were also performed to determine the theoretical UV/visible absorbance maxima, and these data are shown in Table 4. The electronic transitions having the highest oscillator strength are typically from the germanium–germanium single-bond-based HOMO to three orbitals localized on the phenyl groups that correspond to the LUMO+1, LUMO+2, and LUMO+3. The HOMO, LUMO, and LUMO+1 orbitals for digermane 1 are depicted in Figure 6. The LUMO shown in Figure 6b is an antibonding orbital localized along the germanium–germanium bond. Figure 6e and f illustrate the LUMO and LUMO+1, respectively, with the germanium–germanium bond directed into the page.

As found in other investigations, the LUMO and LUMO+*n* orbitals are essentially degenerate, and so several electronic transitions involving the LUMO and the next two or three energy levels are typically observed. A calculated spectrum of the Buⁱ₃GeGePh₃ (4) is shown in Figure 7, which has four predicted absorbance maxima at 242, 249, 252, and 257 nm, with that at 242 nm being the most intense. As indicated by the data in Table 4, the experimental absorbance maximum for 4 was observed at 244 nm, and there is excellent agreement between the calculated and observed λ_{\max} values for the other

seven digermanes as well. Of the eight digermanes investigated, only 7, which contains phenyl substituents on each of the two germanium atoms, has a significant contribution to the UV/visible spectra from the HOMO → LUMO electronic transition.

We were unable to obtain X-ray quality crystals of (C₁₈H₃₇)₃GeGePh₃ (6) for a structural analysis; however, we generated a calculated structure from the DFT computations, which is illustrated in Figure 8. This structure is one of several with a similar energy minimum that differ only in the conformation of the octadecyl groups. The calculated Ge–Ge bond distance is 2.492 Å, which is similar to the crystallographic distance found in most digermanes.^{1,15–18} The average C–Ge–C and C–Ge–Ge bond angles about the octadecyl-substituted germanium atom Ge(2) are 109.8° and 109.1°, respectively, while the C–Ge–C and C–Ge–Ge bond angles about the phenyl-substituted Ge(1) atom are 107.8° and 111.1°, respectively. The average Ge–C distances at Ge(1) and Ge(2) are 1.984 and 1.998 Å. These metric parameters also match closely with those found in digermanes that have been crystallographically characterized. The calculated geometry about Ge(2) in 6 is very similar to that in Buⁿ₃GeGePh₃ (2) ($d_{\text{Ge–Ge}} = 2.4212(8)$ Å)¹⁸ in that the first four carbon atoms of the octadecyl chain are arranged in a similar fashion to the *n*-butyl groups in 2, while the remaining 14 atoms of the octadecyl chain are directed outward away from the Ge–Ge bond.

In conclusion, we have prepared the four new digermanes Buⁱ₃GeGePh₃ (3), Hexⁿ₃GeGePh₃ (5), (C₁₈H₃₇)₃GeGePh₃ (6), and Bu^tMe₂GeGePh₃ (8) starting from the corresponding germanes R₃GeH (R = Buⁱ (12), Hexⁿ (13), C₁₈H₃₇ (14)) or the chloride BuⁿMe₂GeCl. The X-ray crystal structures of 3 and 8 were obtained, and these compounds have Ge–Ge single-bond distances of 2.4410(5) and 2.4255(3) Å, where the former value is an average of two crystallographically independent molecules. These four digermanes and the four previously synthesized digermanes Me₃GeGePh₃ (1),

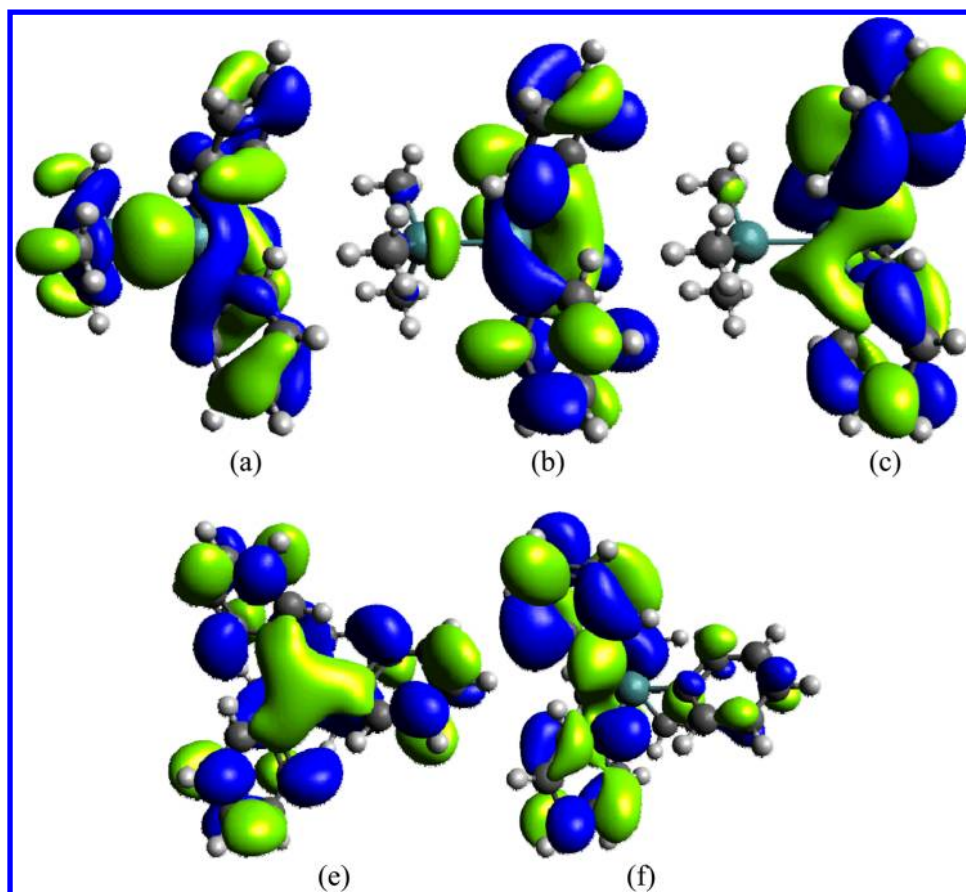


Figure 6. (a) HOMO, (b) LUMO, and (c) LUMO + 1 orbitals computed for species $\text{Me}_3\text{GeGePh}_3$ (1). (e and f) LUMO and LUMO + 1, respectively, with the Ge-Ge bond directed into the page. The LUMO+2 and LUMO+3 are similar to the LUMO+1.

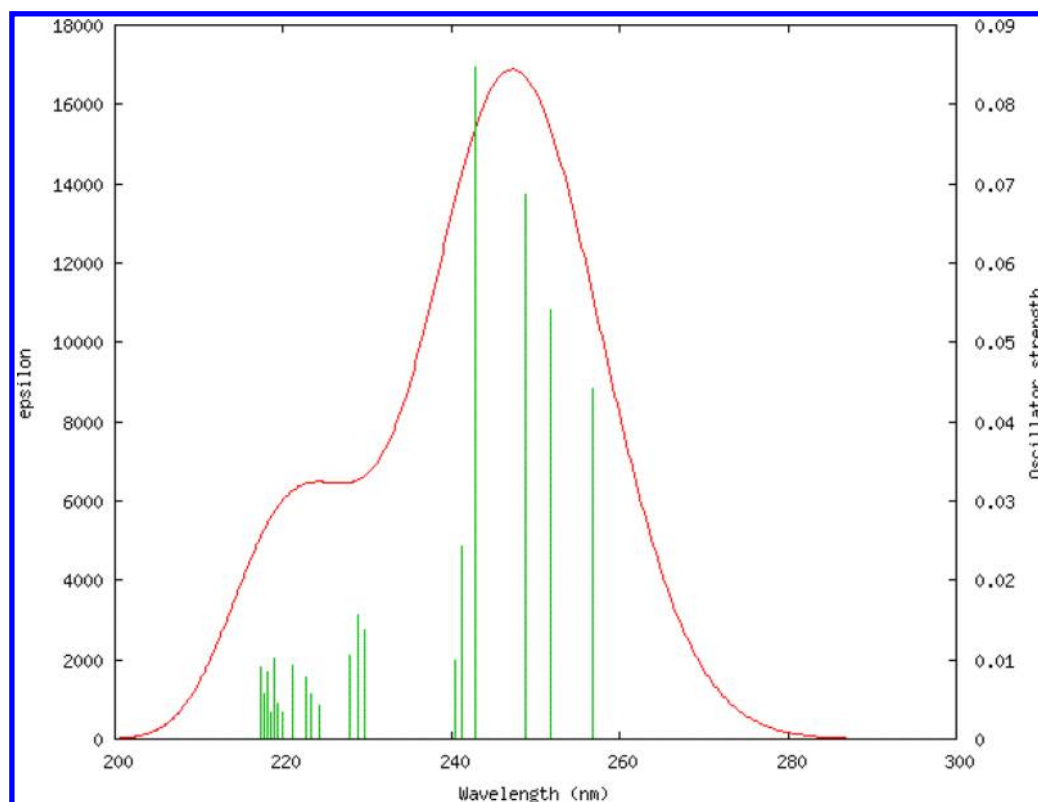


Figure 7. Calculated UV/visible spectrum of $\text{Bu}_3\text{GeGePh}_3$ using time-dependent DFT computations.

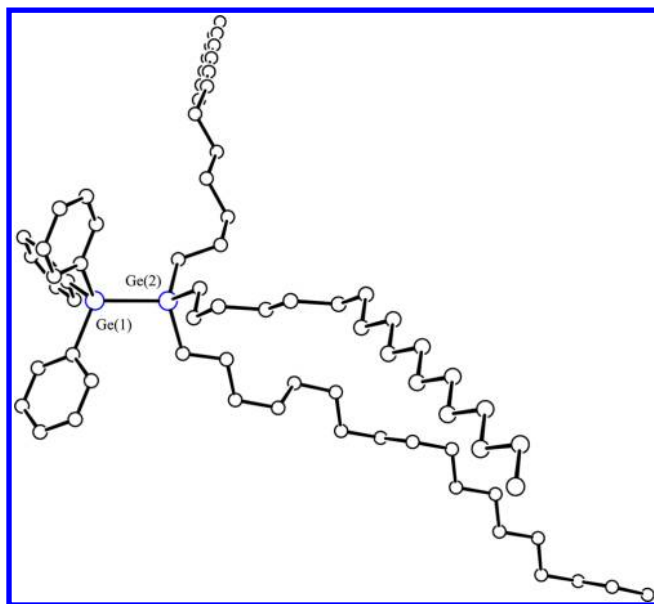


Figure 8. Calculated structure of $(C_{18}H_{37})_3GeGePh_3$ (**6**) using time-dependent DFT computations.

$Bu^n_3GeGePh_3$ (**2**), $Bu^s_3GeGePh_3$ (**4**), and $PhMe_2GeGePh_3$ (**7**) were characterized by cyclic, differential pulse, and linear sweep voltammetry. Each of the digermanes **1–8** exhibits a single irreversible oxidation wave in their cyclic voltammograms. Alteration of the substituent pattern at one germanium atom in these molecules resulted in variation of the observed oxidation potentials with a trend that corresponds to the inductive electron-donating ability of these substituents. In general, digermanes having more highly inductively donating substituents were found to be easier to oxidize, resulting from the destabilization of the HOMO in these molecules, than those having less donating substituents.

Density functional theory calculations were also performed on these molecules, and the theoretical results were compared to the electrochemical data. The DFT findings indicate that the frontier orbitals among the eight digermanes are all similar in energy, and there is very good correlation between the theoretical findings and experimental electrochemical and UV/visible data. As expected, inductively donating substituents at germanium destabilize the HOMO and in general diminish the oxidation potential of the corresponding digermane. The UV/visible spectra of digermanes **1–8** were obtained and range from 230 to 244 nm. The experimental UV/vis data are in excellent agreement with the theoretical data obtained using time-dependent DFT, and the electronic transitions that occur are between the HOMO, which is composed primarily of the germanium–germanium bonding orbitals, and the LUMO or the nearly degenerate LUMO +1, LUMO +2, or LUMO +3, where the latter three MOs are localized on the phenyl substituents.

EXPERIMENTAL SECTION

General Considerations. All reagents were handled under an inert atmosphere of N_2 using standard Schlenk, syringe, and glovebox techniques unless otherwise specified. The compounds $Me_3GeGePh_3$ (**1**),¹⁹ $Bu^n_3GeGePh_3$ (**2**),¹⁷ $Bu^s_3GeGePh_3$ (**4**),²⁰ $PhMe_2GeGePh_3$ (**7**),²⁰ and $K_2[(C_4H_8O_2)_3Ge]$ ^{21,22} were prepared according to literature procedures. The reagent Bu^tMe_2GeCl was purchased from Gelest, Inc., and solutions of Bu^tMgCl , Hex^nMgBr , and $C_{18}H_{37}MgCl$ were purchased from Aldrich. 1H and ^{13}C NMR spectra were recorded at 300 and 75.46 MHz, respectively, using an INOVA Gemini 2000

spectrometer. IR spectra were obtained using a Perkin-Elmer 1720 infrared spectrometer, and UV/visible spectra were recorded using a Hewlett-Packard 8453 diode array spectrometer. Electrochemical data (CV, DPV, LSV, BE) were obtained using a DigiIvy DY2312 potentiostat using a glassy carbon working electrode, a platinum wire counter electrode, and an Ag/AgCl reference electrode in CH_2Cl_2 solution using 0.1 M $[Bu_4N][PF_6]$ as the supporting electrolyte. Bulk electrolyses were conducted in a two-compartment cell using a reticulated vitreous carbon electrode (BASi). Elemental analyses were conducted by Galbraith Laboratories.

Synthesis of Bu^t_3GeH (12**).** To a suspension of $K_2[(C_4H_8O_2)_3Ge]$ (3.756 g, 9.051 mmol) in diethyl ether (100 mL) was added a solution of Bu^tMgCl (10.9 mL, 2.5 M, 27.3 mmol) in THF. The reaction mixture was stirred at room temperature for 2 h followed by the addition of $LiAlH_4$ (1.04 g, 27.3 mmol) using a solid addition funnel. The reaction mixture was stirred for a further 2 h and was then hydrolyzed using an aqueous 25% H_2SO_4 solution. The resulting mixture was filtered, and the filtrate was extracted with diethyl ether (3×25 mL). The Et_2O layer was dried over anhydrous $MgSO_4$ and filtered, and the Et_2O was removed *in vacuo* to yield compound **12** as a colorless liquid (1.817 g, 82%). 1H NMR (25 °C, C_6D_6): δ 3.53 (sept, $J = 2.8$ Hz, 1H, Ge-H), 1.92 (m, 3H, CH), 1.32 (d, $J = 7.0$ Hz, 6H, $-CH_2-$), 0.92 (d, $J = 6.6$ Hz, 18H, $-CH_3$) ppm. ^{13}C NMR (25 °C, C_6D_6): δ 27.3 (CH_3), 26.8 (CH), 26.3 (CH_2) ppm. IR (Nujol): 2010 cm^{-1} (ν_{Ge-H}). Anal. Calcd for $C_{12}H_{28}Ge$: C, 58.81; H, 11.52. Found: C, 58.72; H, 11.58.

Synthesis of Bu^t_3GeCl . To a solution of **12** (1.490 g, 6.085 mmol) in diethyl ether (35 mL) was added $CuCl_2$ (1.64 g, 12.2 mmol). The reaction mixture was stirred at room temperature for 16 h. The mixture was filtered through Celite, and the diethyl ether was removed *in vacuo* to yield Bu^t_3GeCl (1.34 g, 79%) as a colorless liquid. 1H NMR (25 °C, C_6D_6): δ 1.94 (m, 3H, CH), 1.04 (d, $J = 7.0$ Hz, 6H, $-CH_2-$), 0.92 (d, $J = 7.0$ Hz, 18H, $-CH_3$) ppm. ^{13}C NMR (25 °C, C_6D_6): δ 28.1 (CH_2), 27.3 (CH_3), 26.8 (CH) ppm. Anal. Calcd for $C_{12}H_{27}ClGe$: C, 51.56; H, 9.74. Found: C, 51.22; H, 9.89.

Synthesis of $Bu^t_3GeNMe_2$ (9**).** To a solution of Bu^t_3GeCl (1.005 g, 3.596 mmol) in benzene (25 mL) was added $LiNMe_2$ (0.220 g, 4.31 mmol). The reaction mixture was stirred for 18 h and then was filtered through Celite. The volatiles were removed *in vacuo* to yield **9** (0.902 g, 87%) as a pale yellow liquid. 1H NMR (25 °C, C_6D_6): δ 2.57 (s, 6H, $-N(CH_3)_2$), 1.86 (m, 3H, CH), 1.00 (d, $J = 7.0$ Hz, 6H, $-CH_2-$), 0.87 (d, $J = 7.2$ Hz, 18H, $-CH_3$) ppm. ^{13}C NMR (25 °C, C_6D_6): δ 41.2 ($-N(CH_3)_2$), 28.8 (CH_2), 26.9 (CH_3), 25.8 (CH) ppm. Anal. Calcd for $C_{14}H_{33}GeN$: C, 58.35; H, 11.55. Found: C, 58.24; H, 11.77.

Synthesis of $Bu^t_3GeGePh_3$ (3**).** To a solution of **9** (0.503 g, 1.75 mmol) in acetonitrile (20 mL) was added a solution of Ph_3GeH (0.639 g, 2.10 mmol) in acetonitrile (10 mL). The reaction mixture was sealed in a Schlenk tube and heated at 85 °C for 48 h. The volatiles were removed *in vacuo* to yield a light yellow solid. The crude product was distilled in a Kugelrohr oven (125 °C, 0.05 Torr) to remove residual Ph_3GeH , yielding **3** (0.755 g, 79%) as a white solid. 1H NMR (25 °C, C_6D_6): δ 7.69–7.66 (m, 6H, aromatics), 7.21–7.16 (m, 9H, aromatics), 1.90 (m, 3H, CH), 1.25 (d, $J = 6.6$ Hz, 6H, $-CH_2-$), 0.878 (d, $J = 6.6$ Hz, 18H, $-CH_3$) ppm. ^{13}C NMR (25 °C, C_6D_6): δ 135.9 (*o*- C_6H_5), 128.7 (*m*- C_6H_5), 128.6 (*p*- C_6H_5), 27.5 (CH_3), 27.1 (CH), 26.4 (CH_2) ppm. Anal. Calcd for $C_{30}H_{42}Ge_2$: C, 65.75; H, 7.74. Found: C, 65.58; H, 7.64.

Synthesis of Hex^n_3GeH (13**).** To a suspension of $K_2[(C_4H_8O_2)_3Ge]$ (2.500 g, 6.022 mmol) in diethyl ether (100 mL) was added a solution of Hex^nMgBr (9.03 mL, 2.0 M, 18.1 mmol) in THF. The reaction mixture was stirred at room temperature for 1 h followed by the addition of $LiAlH_4$ (0.687 g, 18.1 mmol) using a solid addition funnel. The reaction mixture was stirred for a further 2 h and was then hydrolyzed using an aqueous 25% H_2SO_4 solution. The resulting mixture was filtered, and the filtrate was extracted with diethyl ether (3×15 mL). The Et_2O layer was dried over anhydrous $MgSO_4$ and filtered, and the Et_2O was removed *in vacuo* to yield compound **13** as a colorless liquid (0.317 g, 16%). 1H NMR (25 °C, C_6D_6): δ 4.08 (sept, $J = 3.0$ Hz, 1H, Ge-H), 1.54–1.46 (m, 6H, $-CH_2(CH_2)_4CH_3$), 1.39–1.29 (m, 18H, $-CH_2CH_2CH_2CH_2CH_2CH_3$),

0.93–0.86 (m, 15H, $-\text{CH}_2(\text{CH}_2)_3\text{CH}_2\text{CH}_3$) ppm. ^{13}C NMR (25 °C, C_6D_6): δ 32.2 ($-\text{CH}_2\text{CH}_2\text{CH}_2\text{CH}_2\text{CH}_2\text{CH}_3$), 31.9 ($-\text{CH}_2\text{CH}_2\text{CH}_2\text{CH}_2\text{CH}_2\text{CH}_3$), 26.7 ($-\text{CH}_2\text{CH}_2\text{CH}_2\text{CH}_2\text{CH}_2\text{CH}_3$), 23.0 ($-\text{CH}_2\text{CH}_2\text{CH}_2\text{CH}_2\text{CH}_2\text{CH}_3$), 14.3 ($-\text{CH}_2\text{CH}_2\text{CH}_2\text{CH}_2\text{CH}_2\text{CH}_3$), 12.5 ($-\text{CH}_2\text{CH}_2\text{CH}_2\text{CH}_2\text{CH}_2\text{CH}_3$) ppm. IR (Nujol): 2005 cm^{-1} ($\nu_{\text{Ge-H}}$). Anal. Calcd for $\text{C}_{18}\text{H}_{40}\text{Ge}$: C, 65.66; H, 12.25. Found: C, 65.87; H, 12.37.

Synthesis of $\text{Hex}^n_3\text{GeCl}$. To a solution of **13** (0.351 g, 1.07 mmol) in diethyl ether (20 mL) were added CuCl_2 (0.287 g, 2.13 mmol) and a catalytic amount of CuI (0.006 g, 0.03 mmol). The reaction mixture was stirred at room temperature for 18 h. The mixture was filtered through Celite, and the diethyl ether was removed *in vacuo* to yield $\text{Hex}^n_3\text{GeCl}$ (0.313 g, 81%) as a colorless liquid. ^1H NMR (25 °C, C_6D_6): δ 1.55–1.47 (m, 6H, $-\text{CH}_2(\text{CH}_2)_4\text{CH}_3$), 1.29–1.25 (m, 18H, $-\text{CH}_2\text{CH}_2\text{CH}_2\text{CH}_2\text{CH}_2\text{CH}_3$), 1.10–1.04 (m, 6H, $-\text{CH}_2(\text{CH}_2)_3\text{CH}_2\text{CH}_3$), 0.89 (t, $J = 6.6$ Hz, 9H, $-\text{CH}_3$) ppm. ^{13}C NMR (25 °C, C_6D_6): δ 34.3 ($-\text{CH}_2\text{CH}_2\text{CH}_2\text{CH}_2\text{CH}_2\text{CH}_3$), 32.1 ($-\text{CH}_2\text{CH}_2\text{CH}_2\text{CH}_2\text{CH}_2\text{CH}_3$), 27.2 ($-\text{CH}_2\text{CH}_2\text{CH}_2\text{CH}_2\text{CH}_2\text{CH}_3$), 23.3 ($-\text{CH}_2\text{CH}_2\text{CH}_2\text{CH}_2\text{CH}_2\text{CH}_3$), 14.4 ($-\text{CH}_2\text{CH}_2\text{CH}_2\text{CH}_2\text{CH}_2\text{CH}_3$), 12.7 ($-\text{CH}_2\text{CH}_2\text{CH}_2\text{CH}_2\text{CH}_2\text{CH}_3$) ppm. Anal. Calcd for $\text{C}_{18}\text{H}_{39}\text{GeCl}$: C, 59.44; H, 10.82. Found: C, 59.62; H, 10.89.

Synthesis of $\text{Hex}^n_3\text{GeNMe}_2$ (10**).** To a solution of $\text{Hex}^n_3\text{GeCl}$ (0.313 g, 0.860 mmol) in benzene (50 mL) was added LiNMe_2 (0.053 g, 1.0 mmol). The resulting suspension was stirred for 18 h and then filtered through Celite. The volatiles were removed *in vacuo* to yield **10** (0.266 g, 83%) as a pale yellow liquid. ^1H NMR (25 °C, C_6D_6): δ 2.65 (s, 6H, $-\text{N}(\text{CH}_3)_2$), 1.65–1.60 (m, 6H, $-\text{CH}_2(\text{CH}_2)_4\text{CH}_3$), 1.52–1.32 (m, 18H, $-\text{CH}_2(\text{CH}_2)_3\text{CH}_3$), 1.09–1.04 (m, 6H, $-\text{CH}_2(\text{CH}_2)_3\text{CH}_2\text{CH}_3$), 0.95–0.90 (m, 9H, $-\text{CH}_2(\text{CH}_2)_4\text{CH}_3$) ppm. ^{13}C NMR (25 °C, C_6D_6): δ 42.5 ($-\text{N}(\text{CH}_3)_2$), 37.4 ($-\text{CH}_2\text{CH}_2\text{CH}_2\text{CH}_2\text{CH}_2\text{CH}_3$), 32.8 ($-\text{CH}_2\text{CH}_2\text{CH}_2\text{CH}_2\text{CH}_2\text{CH}_3$), 26.8 ($-\text{CH}_2\text{CH}_2\text{CH}_2\text{CH}_2\text{CH}_2\text{CH}_3$), 23.9 ($-\text{CH}_2\text{CH}_2\text{CH}_2\text{CH}_2\text{CH}_2\text{CH}_3$), 14.6 ($-\text{CH}_2\text{CH}_2\text{CH}_2\text{CH}_2\text{CH}_2\text{CH}_3$), 13.1 ($-\text{CH}_2\text{CH}_2\text{CH}_2\text{CH}_2\text{CH}_2\text{CH}_3$) ppm. Anal. Calcd for $\text{C}_{20}\text{H}_{45}\text{GeN}$: C, 64.52; H, 12.19. Found: C, 64.77; H, 12.25.

Synthesis of $\text{Hex}^n_3\text{GeGePh}_3$ (5**).** To a solution of **10** (0.266 g, 0.710 mmol) in CH_3CN (10 mL) was added a solution of Ph_3GeH (0.240 g, 0.787 mmol) in CH_3CN (10 mL). The reaction mixture was sealed in a Schlenk tube and was heated at 85 °C for 48 h. The volatiles were removed *in vacuo*, and the resulting viscous oil was distilled in a Kugelrohr oven (130 °C, 0.05 Torr) to remove excess Ph_3GeH , yielding **5** (0.194 g, 43%) as a pale yellow liquid. ^1H NMR (25 °C, C_6D_6): δ 7.67–7.65 (m, 6H, $o\text{-C}_6\text{H}_5$), 7.21–7.14 (m, 9H, $m\text{-C}_6\text{H}_5$ and $p\text{-C}_6\text{H}_5$), 1.48–1.42 (m, 6H, $-\text{CH}_2(\text{CH}_2)_4\text{CH}_3$), 1.26–1.16 (m, 24H, $-\text{CH}_2(\text{CH}_2)_4\text{CH}_3$), 0.85–0.81 (m, 9H, $-\text{CH}_2(\text{CH}_2)_4\text{CH}_3$) ppm. ^{13}C NMR (25 °C, C_6D_6): δ 135.7 ($o\text{-C}_6\text{H}_5$), 128.8 ($m\text{-C}_6\text{H}_5$), 128.6 ($p\text{-C}_6\text{H}_5$), 36.2 ($-\text{CH}_2\text{CH}_2\text{CH}_2\text{CH}_2\text{CH}_2\text{CH}_3$), 31.7 ($-\text{CH}_2\text{CH}_2\text{CH}_2\text{CH}_2\text{CH}_2\text{CH}_3$), 26.6 ($-\text{CH}_2\text{CH}_2\text{CH}_2\text{CH}_2\text{CH}_2\text{CH}_3$), 22.9 ($-\text{CH}_2\text{CH}_2\text{CH}_2\text{CH}_2\text{CH}_2\text{CH}_3$), 14.9 ($-\text{CH}_2\text{CH}_2\text{CH}_2\text{CH}_2\text{CH}_2\text{CH}_3$), 14.3 ($-\text{CH}_2\text{CH}_2\text{CH}_2\text{CH}_2\text{CH}_2\text{CH}_3$) ppm. Anal. Calcd for $\text{C}_{36}\text{H}_{54}\text{Ge}_2$: C, 68.39; H, 8.62. Found: C, 68.22; H, 8.55.

Synthesis of $(\text{C}_{18}\text{H}_{37})_3\text{GeH}$ (14**).** To a suspension of $\text{K}_2[(\text{C}_4\text{H}_8\text{O}_2)_3\text{Ge}]$ (6.66 g, 16.0 mmol) in diethyl ether (100 mL) was added a solution of $\text{C}_{18}\text{H}_{37}\text{MgCl}$ (100 mL, 0.5 M, 50.0 mmol) in diethyl ether. The reaction mixture was stirred at room temperature for 2 h followed by the addition of LiAlH_4 (1.61 g, 42.4 mmol) using a solid addition funnel. The reaction mixture was stirred for a further 2 h and was then hydrolyzed using an aqueous 25% H_2SO_4 solution. The resulting mixture was filtered, and the filtrate was extracted with diethyl ether (3 \times 25 mL). The Et_2O layer was dried over anhydrous MgSO_4 and filtered, and the Et_2O was removed *in vacuo* to yield compound **14** as a white solid (7.43 g, 56%). ^1H NMR (25 °C, C_6D_6): δ 4.00 (sept, $J = 2.7$ Hz, 1H, Ge-H), 1.30 (br m, 102H, $-\text{CH}_2(\text{CH}_2)_{16}\text{CH}_3$), 0.91 (t, $J = 6.6$ Hz, 9H, $-\text{CH}_2(\text{CH}_2)_{16}\text{CH}_3$) ppm. ^{13}C NMR (25 °C, C_6D_6): δ 34.4, ($-\text{CH}_2(\text{CH}_2)_{15}\text{CH}_2\text{CH}_2\text{CH}_3$), 30.3 ($-\text{CH}_2(\text{CH}_2)_{14}\text{CH}_2\text{CH}_2\text{CH}_3$), 29.9 ($-\text{CH}_2(\text{CH}_2)_{15}\text{CH}_2\text{CH}_2\text{CH}_3$), 23.2 ($-\text{CH}_2(\text{CH}_2)_{16}\text{CH}_3$), 14.4 ($-\text{CH}_2(\text{CH}_2)_{15}\text{CH}_2\text{CH}_2\text{CH}_3$) ppm. Anal. Calcd for $\text{C}_{54}\text{H}_{112}\text{Ge}$: C, 77.74; H, 13.54. Found: C, 77.82; H, 13.63.

Synthesis of $(\text{C}_{18}\text{H}_{37})_3\text{GeCl}$. To a solution of **14** (6.98 g, 8.37 mmol) in diethyl ether (60 mL) was added CuCl_2 (2.33 g, 1.71 mmol)

and a catalytic amount of CuI (0.28 g, 1.47 mmol). The reaction mixture was stirred at room temperature for 18 h. The mixture was filtered through Celite, and the diethyl ether was removed *in vacuo* to yield $(\text{C}_{18}\text{H}_{37})_3\text{GeCl}$ (6.72 g, 92%) as a pale yellow solid. ^1H NMR (25 °C, C_6D_6): δ 1.34 (br m, 102H, $-\text{CH}_2(\text{CH}_2)_{16}\text{CH}_3$), 0.92 (t, $J = 5.7$ Hz, 9H, $-\text{CH}_2(\text{CH}_2)_{16}\text{CH}_3$) ppm. ^{13}C NMR (25 °C, C_6D_6): δ 32.4, ($-\text{CH}_2(\text{CH}_2)_{15}\text{CH}_2\text{CH}_2\text{CH}_3$), 30.3 ($-\text{CH}_2(\text{CH}_2)_{14}\text{CH}_2\text{CH}_2\text{CH}_3$), 29.9 ($-\text{CH}_2(\text{CH}_2)_{15}\text{CH}_2\text{CH}_2\text{CH}_3$), 23.1 ($-\text{CH}_2(\text{CH}_2)_{16}\text{CH}_3$), 14.4 ($-\text{CH}_2(\text{CH}_2)_{15}\text{CH}_2\text{CH}_2\text{CH}_3$) ppm. Anal. Calcd for $\text{C}_{54}\text{H}_{111}\text{ClGe}$: C, 74.66; H, 12.89. Found: C, 74.80; H, 12.76.

Synthesis of $(\text{C}_{18}\text{H}_{37})_3\text{GeNMe}_2$ (11**).** To a solution of $(\text{C}_{18}\text{H}_{37})_3\text{GeCl}$ (6.409 g, 7.379 mmol) in benzene (60 mL) was added LiNMe_2 (0.46 g, 9.0 mmol). The resulting suspension was stirred for 18 h and then filtered through Celite. The volatiles were removed *in vacuo* to yield **11** (4.19 g, 65%) as a pale yellow solid. ^1H NMR (25 °C, C_6D_6): δ 2.64 (s, 6H, $-\text{N}(\text{CH}_3)_2$), 1.31 (br m, 102H, $-\text{CH}_2(\text{CH}_2)_{16}\text{CH}_3$), 0.92 (t, $J = 6.9$ Hz, 9H, $-\text{CH}_2(\text{CH}_2)_{16}\text{CH}_3$) ppm. ^{13}C NMR (25 °C, C_6D_6): δ 42.5 ($-\text{N}(\text{CH}_3)_2$), 32.4, ($-\text{CH}_2(\text{CH}_2)_{15}\text{CH}_2\text{CH}_2\text{CH}_3$), 30.2 ($-\text{CH}_2(\text{CH}_2)_{14}\text{CH}_2\text{CH}_2\text{CH}_3$), 29.9 ($-\text{CH}_2(\text{CH}_2)_{15}\text{CH}_2\text{CH}_2\text{CH}_3$), 23.1 ($-\text{CH}_2(\text{CH}_2)_{16}\text{CH}_3$), 14.3 ($-\text{CH}_2(\text{CH}_2)_{15}\text{CH}_2\text{CH}_2\text{CH}_3$) ppm. Anal. Calcd for $\text{C}_{56}\text{H}_{117}\text{GeN}$: C, 76.66; H, 13.45. Found: C, 76.33; H, 13.74.

Synthesis of $(\text{C}_{18}\text{H}_{37})_3\text{GeGePh}_3$ (6**).** To a solution of **11** (1.47 g, 1.67 mmol) in CH_3CN (20 mL) was added a solution of Ph_3GeH (0.522 g, 1.71 mmol) in CH_3CN (10 mL). The reaction mixture was sealed in a Schlenk tube and was heated at 85 °C for 48 h. The volatiles were removed *in vacuo*, and the resulting viscous oil was distilled in a Kugelrohr oven (145 °C, 0.07 Torr) to remove excess Ph_3GeH , yielding **6** (0.953 g, 50%) as a pale yellow solid. ^1H NMR (25 °C, C_6D_6): δ 7.48 (m, 6H, $o\text{-C}_6\text{H}_5$), 7.14 (m, 9H, $m\text{-C}_6\text{H}_5$ and $p\text{-C}_6\text{H}_5$), 1.34 (br m, 102H, $-\text{CH}_2(\text{CH}_2)_{16}\text{CH}_3$), 0.92 (t, $J = 6.9$ Hz, 9H, $-\text{CH}_2(\text{CH}_2)_{16}\text{CH}_3$) ppm. ^{13}C NMR (25 °C, C_6D_6): δ 139.1 ($ipso\text{-C}_6\text{H}_5$), 135.5 ($o\text{-C}_6\text{H}_5$), 129.4 ($m\text{-C}_6\text{H}_5$), 128.7 ($p\text{-C}_6\text{H}_5$), 32.4, ($-\text{CH}_2(\text{CH}_2)_{15}\text{CH}_2\text{CH}_2\text{CH}_3$), 30.3 ($-\text{CH}_2(\text{CH}_2)_{14}\text{CH}_2\text{CH}_2\text{CH}_3$), 29.9 ($-\text{CH}_2(\text{CH}_2)_{15}\text{CH}_2\text{CH}_2\text{CH}_3$), 23.2 ($-\text{CH}_2(\text{CH}_2)_{16}\text{CH}_3$), 14.4 ($-\text{CH}_2(\text{CH}_2)_{15}\text{CH}_2\text{CH}_2\text{CH}_3$) ppm. Anal. Calcd for $\text{C}_{72}\text{H}_{126}\text{Ge}_2$: C, 76.04; H, 11.18. Found: C, 76.09; H, 11.22.

Synthesis of $\text{Bu}^t\text{Me}_2\text{GeNMe}_2$ (15**).** To a solution of $\text{Bu}^t\text{Me}_2\text{GeCl}$ (2.000 g, 10.24 mmol) in diethyl ether (25 mL) was added a solution of LiNMe_2 (0.630 g, 12.4 mmol) in diethyl ether (25 mL). The resulting solution was stirred for 18 h and then was filtered through Celite. The Et_2O was distilled off under N_2 , and the resulting residue was taken up in hexane and filtered through Celite. The hexane was distilled off under N_2 to yield **15** (1.600 g, 77%) as a pale yellow liquid. ^1H NMR (25 °C, C_6D_6): δ 2.60 (s, 6H, $-\text{N}(\text{CH}_3)_2$), 0.97 (s, 9H, $-\text{C}(\text{CH}_3)_3$), 0.14 (s, 6H, $-\text{CH}_3$) ppm. ^{13}C NMR (25 °C, C_6D_6): δ 43.4 ($-\text{N}(\text{CH}_3)_2$), 29.1 ($-\text{C}(\text{CH}_3)_3$), 24.2 ($-\text{C}(\text{CH}_3)_3$), -2.3 ($-\text{CH}_3$) ppm. Anal. Calcd for $\text{C}_8\text{H}_{21}\text{GeN}$: C, 47.11; H, 10.40. Found: C, 47.77; H, 9.99.

Synthesis of $\text{Bu}^t\text{Me}_2\text{GeGePh}_3$ (8**).** To a solution of **15** (0.870 g, 4.27 mmol) in CH_3CN (10 mL) was added a solution of Ph_3GeH (1.060 g, 3.476 mmol) in CH_3CN (10 mL). The reaction mixture was sealed in a Schlenk tube and was heated at 85 °C for 48 h. The volatiles were removed *in vacuo*, and the resulting viscous oil was distilled in a Kugelrohr oven (145 °C, 0.07 Torr) to remove excess Ph_3GeH , yielding **8** (1.75 g, 89%) as a pale yellow solid. ^1H NMR (25 °C, C_6D_6): δ 7.63 (d, $J = 7.2$ Hz, 6H, $o\text{-C}_6\text{H}_5$), 7.17–7.14 (m, 9H, $m\text{-C}_6\text{H}_5$ and $p\text{-C}_6\text{H}_5$), 0.97 (s, 9H, $-\text{C}(\text{CH}_3)_3$), 0.39 (s, 6H, $-\text{CH}_3$) ppm. ^{13}C NMR (25 °C, C_6D_6): δ 139.1 ($ipso\text{-C}_6\text{H}_5$), 135.8 ($o\text{-C}_6\text{H}_5$), 128.8 ($m\text{-C}_6\text{H}_5$), 128.6 ($p\text{-C}_6\text{H}_5$), 28.9 ($-\text{C}(\text{CH}_3)_3$), 24.0 ($-\text{C}(\text{CH}_3)_3$), -3.9 ($-\text{CH}_3$) ppm. Anal. Calcd for $\text{C}_{24}\text{H}_{30}\text{Ge}_2$: C, 62.14; H, 6.53. Found: C, 62.70; H, 6.46.

Computational Details. Gaussian 09 was utilized for all computations.⁴² Energy calculations, geometry optimizations, and frequency calculations are performed using the hybrid density functional method including Becke's three-parameter nonlocal-exchange functional⁴³ with the correlation functional of Lee–Yang–Parr, B3LYP.⁴⁴ Final optimizations were performed using the 6-311+G(d,p) basis set.⁴¹ All atomic positions were optimized without geometry constraints to a minimum in the total force. Given that the

HOMO and LUMO energies depend primarily on the local geometry around the Ge atoms, no attempt was made to explore the conformational space for the molecules having long alkyl chains. Frequency calculations were performed at a lower level (6-31G*) to confirm that the stable geometries have real vibrational frequencies. The time-dependent density functional computations, as implemented by Gaussian 09, were utilized to explore the excited manifold and compute the possible electronic transitions and oscillator strengths. GaussSum was used to compute the UV/visible spectra.⁴⁵

X-ray Crystal Structure Determinations. Diffraction intensity data were collected with a Siemens P4/CCD diffractometer. Crystallographic data for the X-ray analysis of **3** and **8** are collected in the Supporting Information (Table S1). The crystal-to-detector distance was 60 mm, and the exposure time was 20 s per frame using a scan width of 0.5°. The data were integrated using the Bruker SAINT software program. Solution by direct methods (SIR-2004) produced a complete heavy atom phasing model consistent with the proposed structures. All non-hydrogen atoms were refined anisotropically by full-matrix least-squares (SHELXL-97). All hydrogen atoms were placed using a riding model. Their positions were constrained relative to their parent atom using the appropriate HFIX command in SHELXL-97.

■ ASSOCIATED CONTENT

📄 Supporting Information

Crystallographic parameters and CIF files giving crystallographic data for **3** and **8**. This material is available free of charge via the Internet at <http://pubs.acs.org>.

■ AUTHOR INFORMATION

Corresponding Author

*E-mail: weinert@chem.okstate.edu.

Notes

The authors declare no competing financial interest.

■ ACKNOWLEDGMENTS

Dedicated to the memory of Prof. Duward F. Shriver (1934–2013). Funding for this work was provided by a CAREER grant from the National Science Foundation (No. CHE-0844758) and is gratefully acknowledged. Computing for this project was partially supported by the OSU High Performance Computing Center at Oklahoma State University, funded in part through instrumentation grant OCI-1126330 by the National Science Foundation.

■ REFERENCES

- (1) Amadoruge, M. L.; Weinert, C. S. *Chem. Rev.* **2008**, *108*, 4253–4294.
- (2) Weinert, C. S. *Dalton Trans.* **2009**, 1691–1699.
- (3) Weinert, C. S. *Comments Inorg. Chem.* **2011**, *32*, 55–87.
- (4) Balaji, V.; Michl, J. *Polyhedron* **1991**, *10*, 1265–1284.
- (5) Miller, R. D.; Michl, J. *Chem. Rev.* **1989**, *89*, 1359–1410.
- (6) Zaitsev, K. V.; Kapranov, A. A.; Opruenko, Y. F.; Churakov, A. V.; Howard, J. A. K.; Tarasevich, B. N.; Karlov, S. S.; Zaitseva, G. S. *J. Organomet. Chem.* **2012**, *700*, 207–213.
- (7) Amadoruge, M. L.; Gardinier, J. R.; Weinert, C. S. *Organometallics* **2008**, *27*, 3753–3760.
- (8) Amadoruge, M. L.; Golen, J. A.; Rheingold, A. L.; Weinert, C. S. *Organometallics* **2008**, *27*, 1979–1984.
- (9) Samanamu, C. R.; Amadoruge, M. L.; Yoder, C. H.; Golen, J. A.; Moore, C. E.; Rheingold, A. L.; Materer, N. F.; Weinert, C. S. *Organometallics* **2011**, *30*, 1046–1058.
- (10) Samanamu, C. R.; Amadoruge, M. L.; Schrick, A. C.; Chen, C.; Golen, J. A.; Rheingold, A. L.; Materer, N. F.; Weinert, C. S. *Organometallics* **2012**, *31*, 4374–4385.

- (11) Mochida, K.; Hodota, C.; Hata, R.; Fukuzumi, S. *Organometallics* **1993**, *12*, 586–588.
- (12) Okano, M.; Mochida, K. *Chem. Lett.* **1990**, 701–704.
- (13) Amadoruge, M. L.; Short, E. K.; Moore, C.; Rheingold, A. L.; Weinert, C. S. *J. Organomet. Chem.* **2010**, *695*, 1813–1823.
- (14) Samanamu, C. R.; Amadoruge, M. L.; Weinert, C. S.; Golen, J. A.; Rheingold, A. L. *Phosphorus, Sulfur, Silicon* **2011**, *186*, XXXXX.
- (15) Samanamu, C. R.; Materer, N. F.; Weinert, C. S. *J. Organomet. Chem.* **2012**, *698*, 62–65.
- (16) Amadoruge, M. L.; DiPasquale, A. G.; Rheingold, A. L.; Weinert, C. S. *J. Organomet. Chem.* **2008**, *693*, 1771–1778.
- (17) Subashi, E.; Rheingold, A. L.; Weinert, C. S. *Organometallics* **2006**, *25*, 3211–3219.
- (18) Párkányi, L.; Kálman, A.; Sharma, S.; Nolan, D. M.; Pannell, K. H. *Inorg. Chem.* **1994**, *33*, 180–182.
- (19) Marchand, A.; Gerval, P.; Soulard, M. H.; Rivière, P.; Satgé, J.; Richelme, S. *J. Organomet. Chem.* **1978**, *162*, 365–387.
- (20) Amadoruge, M. L.; Yoder, C. H.; Conneywerdy, J. H.; Heroux, K.; Rheingold, A. L.; Weinert, C. S. *Organometallics* **2009**, *28*, 3067–3073.
- (21) Cerveau, G.; Chuit, C.; Corriu, R. J. P.; Reyé, C. *Organometallics* **1988**, *7*, 786–787.
- (22) Cerveau, G.; Chuit, C.; Corriu, R. J. P.; Reyé, C. *Organometallics* **1991**, *10*, 1510–1515.
- (23) Cross, R. J.; Glockling, F. J. *J. Organomet. Chem.* **1965**, *3*, 146–155.
- (24) Oshita, J.; Toyoshima, Y.; Iwata, A.; Tang, H.; Kunai, A. *Chem. Lett.* **2001**, 886–887.
- (25) Mack, J.; Yoder, C. H. *Inorg. Chem.* **1969**, *8*, 278–281.
- (26) Anson, C. W.; Thamattoor, D. M. *J. Org. Chem.* **2012**, *77*, 1693–1700.
- (27) Penn, L.; Mallory, F. B. *J. Magn. Reson.* **1975**, *18*, 6–11.
- (28) Miura, K.; Ootsuka, K.; Hosomi, A. *J. Organomet. Chem.* **2007**, *692*, 514–519.
- (29) Dräger, M.; Ross, L. *Z. Anorg. Allg. Chem.* **1980**, *469*, 115–122.
- (30) Hanson, P. J. *Chem. Soc., Perkin Trans. 2* **1984**, 101–108.
- (31) Mochida, K.; Chiba, H. *J. Organomet. Chem.* **1994**, *473*, 45–54.
- (32) Mochida, K.; Chiba, H.; Okano, M. *Chem. Lett.* **1991**, 109–112.
- (33) Mochida, K.; Shimizu, H.; Nanjo, M. *Chem. Lett.* **2000**, 1226–1227.
- (34) Lei, D.; Gaspar, P. P. *Polyhedron* **1991**, *10*, 1221–1225.
- (35) Mochida, K.; Wakasa, M.; Nakadaira, Y.; Sakaguchi, Y.; Hayashi, H. *Organometallics* **1988**, *7*, 1869–1871.
- (36) Mochida, K.; Yoneda, I.; Wakasa, M. *J. Organomet. Chem.* **1990**, *399*, 53–62.
- (37) Wakasa, M.; Yoneda, I.; Mochida, K. *J. Organomet. Chem.* **1989**, *366*, C1–C5.
- (38) Mochida, K.; Kikkawa, N.; Nakadaira, Y. *Chem. Lett.* **1988**, 1089–1092.
- (39) Mazerolles, P.; Manuel, G. *Bull. Soc. Chim. Fr.* **1966**, 327–331.
- (40) Bobbitt, K. L.; Maloney, V. M.; Gaspar, P. P. *Organometallics* **1991**, *10*, 2272–2777.
- (41) Francl, M. M.; Pietro, W. J.; Hehre, W. J.; Binkley, J. S.; Gordon, M. S.; DeFrees, D. J.; Pople, J. A. *J. Chem. Phys.* **1982**, *77*, 3654–3665.
- (42) Frisch, M. J.; Trucks, G. W.; Schlegel, H. B.; Scuseria, G. E.; Robb, M. A.; Cheeseman, J. R.; Montgomery, J. A., Jr.; Vreven, T.; Kudin, K. N.; Barant, J. C.; Millam, J. M.; yengar, S. S.; Tomasi, J.; Barone, V.; Mennucci, B.; Cossi, M.; Scalmani, G.; Rega, N.; Petersson, G. A.; Nakatsuji, H.; Hada, M.; Ehara, M.; Toyota, K.; Fukuda, R.; Hasegawa, J.; Ishida, M.; Nakajima, T.; Honda, Y.; Kitao, O.; Nakai, H.; Klene, M.; Li, X.; Knox, J. E.; Hratchian, H. P.; Cross, J. B.; Bakken, V.; Adamo, C.; Jaramillo, J.; Gomperts, R.; Stratmann, R. E.; Yazyev, O.; Austin, A. J.; Cammi, R.; Pomelli, C.; Ochterski, J. W.; Ayala, P. Y.; Morokuma, K.; Voth, G. A.; Salvador, P.; Dannenberg, J. J.; Zakrzewski, V. G.; Dapprich, S.; Daniels, A. D.; Strain, M. C.; Farkas, O.; Malick, D. K.; Rabuck, A. D.; Raghavachari, K.; Foresman, J. B.; Ortiz, J. V.; Cui, Q.; Baboul, A. G.; Clifford, S.; Cioslowski, J.; Stefanov, B. B.; Liu, G.; Liashenko, A.; Piskorz, P.; Komaromi, I.; Martin, R. L.; Fox, D. J.; Keith, T.; Al-Laham, M. A.; Peng, C. Y.;

- Nanayakkara, A.; Challacombe, M.; Gill, P. M. W.; Johnson, B.; Chen, W.; Wong, M. W.; Gonzalez, C.; Pople, J. A. *Gaussian 03*, Revision C.02; Gaussian Inc.: Wallingford, CT, 2004.
- (43) Becke, A. D. *J. Chem. Phys.* **1993**, *98*, 5648–5652.
- (44) Lee, C.; Yang, W.; G., P. R. *Phys. Rev.* **1988**, *B 37*, 785–789.
- (45) O'Boyle, N. M.; Tenderhold, A. M.; Langer, K. M. *J. Comput. Chem.* **2008**, *29*, 839–845.